Jestr

Journal of Engineering Science and Technology Review 16 (4) (2023) 153 - 170

Research Article

JOURNAL OF
Engineering Science and Technology Review

www.jestr.org

Inversion of Nitrogen Content in Winter Wheat Based on Unmanned Aerial Vehicle Hyperspectral Fractional Differentiation

Ma Xiaoxiao[1, 2,*], Chen Peng[3], Li Changchun[4], Cui Yingying[3] and Joël Van Cranenbroeck[5]

[1]*School of Civil Engineering and Architecture, Zhengzhou Vocational University of Information and Technology, Zhengzhou 450046, China*
[2]*Henan Province Engineering Research Center of Intelligent Green Construction, Zhengzhou 45004, China*
[3]*Xiangcheng City Planning Technology and Exhibition Center, Zhoukou 466200, China*
[4]*School of Surveying and Land Information Engineering, Henan Polytechnic University, Jiaozuo 454003, China*
[5]*Cgeos – Creative Geosensing Srl, Rue du Tienne de Mont, 11, 5530 Mont (Yvoir), Belgium*

Received 30 May 2023; Accepted 21 August 2023

Abstract

Crop nitrogen content inversion based on UAV (Unmanned Aerial Vehicle) hyperspectral data is vital for addressing global food supply challenges. Many studies have estimated nitrogen content via simple linear regression using a single vegetation index, multiple vegetation indices, hyperspectral representation, and simple structural transformation. Utilizing UAV hyperspectral data of the winter wheat canopy and leveraging the benefits of fractional differential processing to enhance spectral details, traditional hyperspectral vegetation indices were established, and characteristic parameters derived from spectral position and canopy area were extracted. Then, winter wheat plant nitrogen content models with different spectral information characteristics were highlighted, optimally selected and verified. Results reveal that when the original canopy spectrum is processed using the fractional differential, the association between hyperspectral reflectance and nitrogen levels in winter wheat plants can be effectively enhanced. Fractional differential spectra represent outstanding effects on refining spectral details. The findings provide valuable insights into the potential of hyperspectral fractional differential spectra to enhance the precision of nitrogen estimation in winter wheat.

Keywords: Fractional differential, Spectral position and area, Optimal subset regression, Model, Plant nitrogen content

1. Introduction

Recently, the increasing risk of global crop yield reduction has aggravated the instability and uncertainty of the global food supply. Food security is a fundamental issue related to human survival. According to data from the Food and Agriculture Organization of the United Nations, the global count of individuals facing prolonged food shortages has increased since 2015. At present, wheat remains the most widely distributed food crop on a global scale and holds significant importance as a food crop in China. Analyzing winter wheat's phenotypic characteristics and growth mechanisms, along with timely awareness of its planting status, is essential for the management of winter wheat field growth and optimization of planting patterns, the development of reasonable and efficient fertilization strategies, and the promotion of efficient and high yield of wheat crops, as well as the further exploration of winter wheat production potential [1–4].

Nitrogen is vital for crop development and significantly affects the quality, yield, and growth of winter wheat [5–7]. Nitrogen nutrition status is a key indicator for evaluating winter wheat growth, improving quality, and increasing yield. Nitrogen deficiency in winter wheat affects chlorophyll and protein synthesis, weakens photosynthesis, and hinders the production of dry materials. In the case of severe nitrogen deficiency, the cell differentiation of crops stops, and the tillering ability and root system are weakened. When winter wheat has an excessive nitrogen content, there is a rise in ineffective tillers. Furthermore, the plants become extremely dense. It results in poor light transmission, low fruiting rate, and maturity delayed. However, it sharply increases the probability of plant diseases and insect pests. Therefore, the scientific and accurate management of nitrogen fertilizer prescriptions can optimize the supply and demand of nitrogen for crops and improve the nutrient utilization rate while maintaining high yields [8–13].

On this basis, many experts and scholars have extensively researched the nondestructive monitoring of crop phenotypes by hyperspectral remote sensing. Yue J et al. [14] estimated agricultural parameters such as crop biomass using hyperspectral data obtained by UAVs (Unmanned Aerial Vehicle System). Kefauver et al. [15] studied the models of estimating barley yield and nitrogen use efficiency by multiple airborne and ground spectrometers and found that the estimation accuracy can be enhanced by combining UAV (Unmanned Aerial Vehicle) and ground data. Liu C H et al. [16] used an ASD Field Spec3 ground-based spectrometer and ten spectral preprocessing methods combined with partial least squares (PLSR), back-propagation neural network, and random forest (RF) algorithm to model nitrogen nutrition in winter wheat. The findings indicated that RF + convolution smoothing had the best modeling accuracy. Klem K et al. [17] used remote sensing data to investigate the interaction between wheat's water deficit and nitrogen nutrition level and found that the total N absorption of wheat grain can be effectively estimated by transforming chlorophyll absorption and reflection index (TCARI)/optimizing soil adjusted vegetation index (OSAVI), especially the influence of water.

*E-mail address: mxx1010@126.com
ISSN: 1791-2377
doi:10.25103/jestr.164.20

These factors should be considered when estimating the protein in wheat grain. Katherine Frels et al. [18] obtained canopy spectral reflectance data of 299 wheat varieties in Ithaca and calculated 28 vegetation indices according to the data. The vegetation index of Maccioni could predict the nitrogen use efficiency of durum wheat and could be used in wheat variety breeding. Using UAV-based hyperspectral remote sensing data, Feng S et al. [19] employed the extreme learning algorithm to predict the LNC of rice. The model accuracy R^2 reached 0.81. Lukas Prey et al. [20] found that the milk ripe stage was the best time to assess the nitrogen use efficiency of wheat. The spectral index derived from the water and red bands provided a more accurate estimation than that from the near-infrared and visible bands. Liu H et al. [21] used ground and UAV-borne hyperspectral equipment to gather data on the hyperspectral remote sensing and nitrogen nutrition index (NNI) of winter wheat at various growth stages and indicated that the green band, red edge, and near-infrared band were responsive to the NNI of winter wheat, suggesting their potential for NNI estimation. Pullanagari et al. [22] proposed that a model utilizing a one-dimensional convolutional neural network surpassed the PLSR and Gaussian process regression model for evaluating the canopy nitrogen concentration. Iman Tahmasbian et al. [23] utilized hyperspectral images and a PLSR algorithm to assess the nitrogen level in wheat leaves, achieving a coefficient of determination that exceeded 0.9. Phuoang-Phi et al. [24] estimated the rice yield in the Mekong Delta of Vietnam utilizing multiperiod Sentinel-1 satellite data. Burns B W et al. [25] utilized multispectral and thermal sensors to acquire weekly remote sensing data from corn fields and formulated a model to evaluate nitrogen content under six vegetation indices. The GNDVI (Green Normalized Difference Vegetation Index) and RENDVI (Red Edge NDVI) strongly correlated with the nitrogen fertilizer treatment.

The abovementioned study results indicate that nitrogen estimation has been completed using a single vegetation index or multiple vegetation indices or hyperspectral representation and simple structural transformation based on simple linear regression. However, the hyperspectral high-throughput multiband characteristics of UAVs have not been fully utilized. Meanwhile, reflecting the original spectrum or integering order differential spectrum is mainly applied in current crop monitoring, but the original spectrum retains background and other noise, and integering order differential can overprocess the spectrum to affect the telemetry accuracy [26–35].

Therefore, taking advantage of the advantages of hyperspectral fractional differential spectroscopy and utilizing UAV hyperspectral data of winter wheat canopy, this research utilized fractional differential as an extension of integer differential to weaken the interference of soil background and other noise, refine spectral information, highlight spectral differences in crop physiological states, explore inversion models for nitrogen level in winter wheat plants at various growth stages, and conduct multidimensional spectral analysis first as a whole and then in detail. The study utilized the Pearson correlation coefficient to optimize the response of fractional differentiation and original spectra to nitrogen content in winter wheat plants, subsequently selecting the most relevant and statistically significant features. Traditional vegetation indices were constructed using hyperspectral information, and highly significant features were selected based on spectral location and area features. Based on full subset regression analysis, 10-fold cross-validation and other methods were used to screen the optimal subset model for nitrogen level in winter wheat plants of different growth stages and verify its accuracy. In this manner, the precision of estimating nitrogen content in winter wheat can be improved, further providing a basis for scientific and precise prescription of nitrogen fertilizers.

2. Materials and Methods

2.1 Study area

The investigation was conducted in Jiaozuo City, Henan Province of China (the comprehensive experimental base of winter wheat at the eastern entry point of Nandao Village), and it has flat terrain, fertile lands, abundant sunshine, and four distinct seasons. With a yearly temperature averaging between 12.8 °C and 15.5 °C and yearly rainfall of around 600 mm, the region is characterized by a temperate monsoon climate.

The study area included four rows, with 12 plots in each row, totaling 48 plots, 38.9 m in south-to-north length and 66 m in east-to-west length. Each plot covered an area of 9 m × 4 m. Field management work included weeding, earthing-up, and irrigation. Fertilizer application was categorized into base fertilizer application and topdressing. UAV remote sensing data were acquired and sampled synchronously with field data. The experimental data were collected from winter wheat plants during the jointing, booting, flowering, and fillnter wheat in 2021. The experimental data mainly included the canopy hyperspectral and nitrogen content data of UAVs (with particular emphasis on the jointing and filling stages of winter wheat).

2.2 Acquisition and preprocessing of UAV remote sensing data

In this study, an eight-rotor wing UAV served as the primary platform (net weight: 4.2 kg, load capacity: 6 kg, flight duration: 20 minutes) and was fitted with a high-definition digital camera and airborne imaging spectrometer to obtain remote sensing data of the UAV. The data acquisition was for stable solar radiation and cloudless clear weather. The parameters of the airborne imaging spectrometer are listed in Table 1. The data were preprocessed and spliced via built-in hyperspectral software. ArcGIS was employed to extract the average spectral reflectance for each plot. Finally, the spectral data in CSV (Comma Separate Values) format were exported. For instance, the hyperspectral curve of the UAV at the jointing stage is the typical vegetation curve in Figure 1.

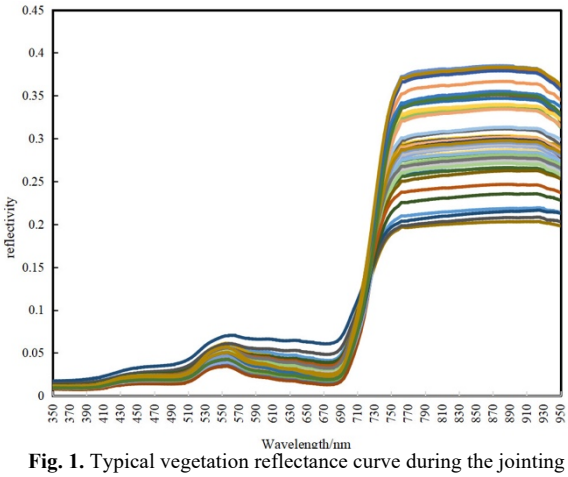

Fig. 1. Typical vegetation reflectance curve during the jointing stage

Table 1. Parameters of the airborne imaging spectrometer

Instrument specification	Technical parameter
Spectral range	450–950 nm
Sampling interval	4 nm
Spectral resolution	8 nm@532 nm
Spectral channel	125
Spectral sampling (physical)	1.05 nm/pix@450 nm; 4.54 nm/pix@650 nm; 8.13 nm/pix@900 nm;
Wavelength precision	±2.5 nm/±4.5 nm
Detector	Si CCD
Digital resolution	12 bit
Measurement time	<100 μs
Hyperspectral imaging speed	5 cubes/s
Spatial resolution	100 megapixels
Spectral output	2500 spectra/cube

2.3 Determination of nitrogen content in winter wheat plants

Random sampling was conducted in each plot. Twenty typical winter wheat plants were selected and preserved in sealed plastic bags. After returning to the laboratory, the winter wheat was divided into different organ groups, such as stems, leaves, and ears, which were inactivated at 105 °C for 30 minutes and then dried at 75 °C until weight stabilization. Then, the mass of dry materials was recorded. The Kjeldahl approach was employed to determine the total nitrogen content in each winter wheat component. The effect of ear nitrogen on plant nitrogen content should be considered during the flowering and filling stages. Here, the plant nitrogen content (%) was calculated as follows:

$$\begin{aligned} Plant\ nitrogen\ content = {} & (Stem\ nitrogen\ content \times Stem\ biomass \\ & + Leaf\ nitrogen\ content \times Leaf\ biomass \\ & + Ear\ nitrogen\ content \times Ear\ biomass) \Big/ \begin{matrix} (Leaf\ biomass \\ + Stem\ biomass \\ + Ear\ biomass) \end{matrix} \end{aligned} \quad (1)$$

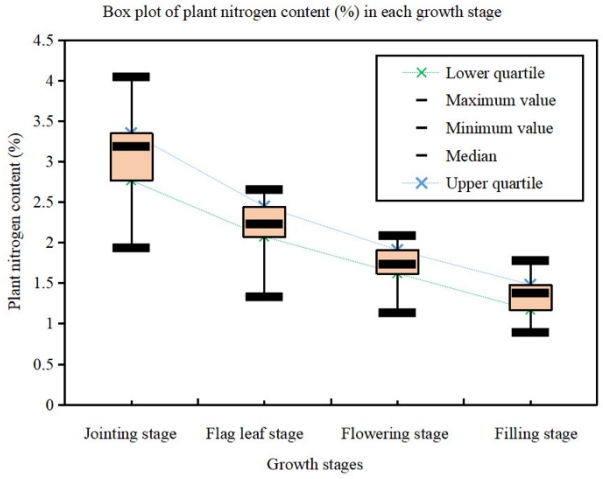

Fig. 2. Box plot of nitrogen content in winter wheat

The box plot of nitrogen level in winter wheat plants at four key growth stages is shown in Figure 2.The box plot visually shows the spacing between the upper and lower quartiles, with the height of the box symbolizing this spacing. A smaller spacing indicates a higher concentration of data, while a larger spacing indicates a higher dispersion of data. The rectangular height of the box during the jointing and filling stages of winter wheat was lower than that at the other two stages, indicating that the data were concentrated. The central line within the box marks the median of the data, reflecting the average value of the sampled set. Notably, during the jointing phase of winter wheat, the position of this median was elevated compared to its counterparts in the other three phases, suggesting a higher nitrogen content during this stage. In summary, the nitrogen content level of wheat showed an overall downtrend with the advancement of the growth period and the transfer and growth of aboveground and underground materials.

2.4 Data processing method

2.4.1 Fractional differential processing

Fractional differentials are currently widely used in image signals and other fields and are an extension of integral differentials; however, they can amplify subtle hyperspectral changes, effectively remove background noise, and obtain detailed information. With the development of the signal analysis field, the commonly used fractional differential forms are the methods of Grünwald–Letnikov, Caputo, and Riemann–Liouville [36-38]. Here, the Grünwald–Letnikov differential definition was adopted to process hyperspectral data as follows:

$$\frac{d^{\alpha} f(\lambda)}{d\lambda^{\alpha}} \approx f(\lambda) + (-\alpha) f(\lambda - 1) + \frac{(-\alpha)(-\alpha+1)}{2} f(\lambda - 2) + \ldots + \frac{\Gamma(-\alpha+1)}{n!\Gamma(-\alpha+1)} f(\lambda - n) \quad (2)$$

Where Γ represents the Gamma function, λ denotes the spectral wavelength, n represents the upper and lower finite difference, and α is the number of orders. When α = 0, 1, or 2, it refers to the original, first-order, or second-order, differential spectrum. When α takes a decimal value, it is a fractional differential form.

2.4.2 Selection of hyperspectral vegetation indices

Twenty-two hyperspectral vegetation indices associated with plant nitrogen level were chosen (Table 2).

2.4.3 Deriving characteristic parameters from the spectral location and coverage of winter wheat

According to the differential analysis of hyperspectral data, characteristic parameters were identified with spectral location and area (Table 3) [26]. Previous studies have shown that variations in spectral positions and area changes can be used to assess plant growth conditions under physiological stress [39,40].

Table 2. Hyperspectral vegetation indices

Vegetation index	Formula
R	$R_{622:778}$ mean
G	$R_{494:574}$mean
B	$R_{454:490}$mean
NIR	$R_{782:950}$ mean
R'	$R_{622:778}$ first-order derivative mean
G'	$R_{494:574}$ first-order derivative mean
B'	$R_{454:490}$ first-order derivative mean
NIR'	$R_{782:950}$ first-order derivative mean
Green Red Vegetation Index (GRVI)	GRVI=NIR/G-1

The Second Modified SAVI (MSAVI2)	$MSAVI2=(2NIR+1-((2NIR+1)^2-8(NIR-RED))^{0.5})/2$
Optimization of Soil-Adjusted Vegetation Index (OSAVI)	$OSAVI=(1+0.16)(NIR-RED)/(NIR+RED+0.16)$
Enhanced Vegetation Index (EVI)	$EVI=(NIR-RED)/(NIR+6RED-7.5B+1)$
Carter6	R_{550}
D1	R_{730}/R_{706}
Datt2	R_{850}/R_{710}
EGFN	$(\max(R_{650:750})-\max(R_{500:550})(\max(R_{650:750})+\max(R_{500:550}))$
EGFR	$\max(R_{650:750})/\max(R_{500:550})$
GMI1	R_{750}/R_{550}
Derivative Spectral Normalized Vegetation Index (FDNDVI)	$FDNDVI=(R'NIR-R'R)/(R'NIR+R'R)$
Derivative Spectra Difference Vegetation Index (FDDVI)	$FDDVI=R'NIR-R'R$
Derivative Spectral Ratio Vegetation Index (FDRVI)	$FDRVI=R'NIR/R'R$
Derivative Spectra Optimization Soil Adjusted Vegetation Index (FDOSAVI)	$FDOSAVI=(R'NIR-R'R)/(R'NIR+R'R+0.16)$

Table. 3. Characteristic parameters based on the spectral position and area

Variable name	Code	Definition
Blue edge amplitude	D_b	Maximum value of the first-order derivative spectrum (490–530 nm)
Blue edge position	λ_b	Wavelength corresponding to the maximum value of the first-order derivative spectrum (490–530 nm)
Blue edge area	SD_b	Integral of the first-order derivative spectrum (490–530 nm)
Yellow edge amplitude	D_y	Maximum value of the first-order derivative spectrum (560–640 nm)
Yellow edge position	λ_y	Wavelength corresponding to the maximum value of the first-order derivative spectrum (560–640 nm)
Yellow edge area	SD_y	Integral of the first-order derivative spectrum (560–640 nm)
Red edge amplitude	D_r	Maximum value of the first-order derivative spectrum (680–760 nm)
Red edge position	λ_r	Wavelength corresponding to the maximum value of the first-order derivative spectrum (680–760 nm)
Red edge area	SD_r	Integral of the first-order derivative spectrum (680–760 nm)
Green peak reflectance	ρ_g	Maximum band reflectance (510–560) nm
Green peak position	λ_g	Wavelength corresponding to the maximum band reflectance (510–560 nm)
Green peak area	SD_g	Area circled by the original spectral curve (510–560 nm)
Red valley reflectance	ρ_r	Minimum band reflectance (650–690 nm)
Red valley position	λ_o	Wavelength corresponding to the minimum band reflectance (650–690 nm)

2.5 Modeling method and accuracy evaluation indices

2.5.1 Adjusted R^2 and all subset regression analyses

In multilinear regression, the addition of independent variables, regardless of their significance, would lead to a gradual increase in the model's R^2. This occurrence can be attributed to the negative correlation between the residual sum of squares (RSS) and the independent variables (i.e., decreased with the increase in independent variables). This phenomenon results in "overfitting", further leading to the accidental increase in data. However, the adjusted R^2 (R^2_{adj}) considered the influences of both the number of samples and independent variables. Hence, R^2_{adj} presented higher authenticity and reliability than R^2. All subset regression analyses based on R^2_{adj} were combined to model all features of R^2_{adj}. The optimal model was determined based on the maximum value of R^2_{adj}.

2.5.2 K-fold cross-validation (K-fold CV) and all subset optimal regression analyses

In machine learning, cross-validation is highly universal for verifying the deviation and variance of the model and is not limited to the model itself. The K-fold cross-validation algorithm is as follows:

1) The samples are randomly divided into K approximately sized folds;

2) The samples of the i-th fold ($1 \leqslant i \leqslant k$) are classified into the validation set, while the remaining samples constitute the training set to develop the model;

3) The mean validation error of K models is taken as the overall model validation error.

The advantage of this method over leave-one-out cross-validation lies in the small calculated quantity, as the latter needs to calculate n times while this method only needs k times (i.e., tenfold in general). Similarly, leave-one-out cross-validation tends to result in "overfitting", which can be effectively avoided by K-fold cross-validation.

In this research, the tenfold cross-validation model was compared with the R^2_{adj}-based optimal model with the minimum deviation as the basis.

2.5.3 Akaike information criterion

The Akaike information criterion measures a model's complexity and fits the data based on the concept of entropy, aiming to seek the model that best explains data and contains the fewest free parameters. A smaller AIC value indicates a superior model, and it is expressed as:

$$AIC = n\ln(\frac{\sum S_p^2}{m}) + 2(k+1) \tag{3}$$

Where n denotes the number of model samples, m indicates the model's degree of freedom, k stands for the number of variables, and S^2_p is the mean square residual.

2.5.4 Evaluation indices for model performance

The evaluation of model accuracy was based on three indices: the coefficient of determination (R^2), root mean-square error (*RMSE*), and normalized root mean-square error (*nRMSE*)[29]. These indices quantify the accuracy of the model and can be presented as follows:

$$R^2 = \frac{(\sum_{i=1}^{n} y_i - \bar{y})^2}{(\sum_{i=1}^{n} x_i - \bar{y})^2} \tag{4}$$

$$RMSE = \sqrt{\frac{\sum_{i=1,j=1}^{n} (x_i - y_j)^2}{n}} \tag{5}$$

$$nRMSE = \sqrt{\frac{\sum_{i=1,j=1}^{n} (x_i - y_j)^2}{n}} \Big/ \bar{y} \tag{6}$$

Where x_i represents the actual value of plant nitrogen level; y_j represents the estimated value of plant nitrogen level; $\bar{y}$ signifies the average nitrogen level; and n denotes the sample size.

This study established a nitrogen level model of winter wheat plants at two typical growth stages: the jointing and filling stages, for estimation based on UAV hyperspectral data.

3. Results Analysis and Discussion

3.1 Correlation analysis between canopy spectrum and winter wheat plant nitrogen content

3.1.1 Correlation analysis between the original canopy spectrum and winter wheat plant nitrogen content (N%)

In this research, 48 samples from the jointing and filling stages of winter wheat underwent correlation analysis with plant nitrogen content (N%). The findings are depicted in Figures 3a and 3b. According to Figure 3a, at the jointing stage, canopy spectra correlation coefficients (sampling interval: 4 nm) had absolute values in the 734 – 758 nm and 930 – 950 nm ranges. The N% was between 0.578 and 0.605, reaching the first 13 positions at the highly significant level (P<0.001). Figure 3b shows the trends for the maturation stage. The absolute values of the correlation coefficients of the canopy spectra (sampling interval: 4 nm) were 402 nm and between 410nm and 454 nm. The N% was between 0.519 and 0.535, reaching the first 13 positions at the highly significant level (P<0.001).

(a) Jointing stage (b) Filling stage

(Note: The numbers in the figure are absolute values of correlation coefficients. The closer the number is to 1, the higher the correlation, the same below).

Fig. 3. Correlation coefficient matrix diagram of the original canopy spectra of winter wheat during the jointing and filling stages

3.1.2 Correlation between the canopy fractional spectrum and nitrogen content (N%) of winter wheat plants

The spectral data of 48 samples (350–950 nm) at each growth stage were subjected to 0- to 2.4-order fractional differential processing with 0.2 as the order. Then, we conducted a correlation analysis between the fractional differential spectrum orders for the 48 samples across different growth stages and the winter wheat plant nitrogen content (Figures 4 and 5). A highly significant positive correlation exists between the 0-order spectrum (original spectrum) and winter wheat plant nitrogen at 726–950 nm (P<0.001) (Figure 4). Combined with the trends (Figure 5), when the order increased from 0 to 1.0 at the jointing stage, fractional differential spectra showing highly significant correlations with plant nitrogen first increased and then decreased. The normal distribution trend was mainly in 610–682, 714–798, 802–898, and 902–950 nm. As the order increased from 1.2 to 2.4, the number of fractional differential spectra showing highly significant correlations with plant nitrogen gradually decreased, while the wavebands passing the 0.1% significance test fluctuated more prominently. Furthermore, the band intervals were increasingly dispersed. Figures 4 and 5 also show the trends for the filling stage. The order increased from 0 to 2.4. Furthermore, the number of fractional differential spectra also showed highly significant correlations. The plant nitrogen gradually decreased. In the order range between 0 and 1.0, such fractional differential spectra were mainly concentrated in 350–398, 402–798, 502–598, 602–698, and 702–718 nm. When the order was between 1.0 and 2.4, the bands passing the 0.1% significance test fluctuated more intensely. The highly significant band intervals tended to a dispersed state without evident characteristic laws.

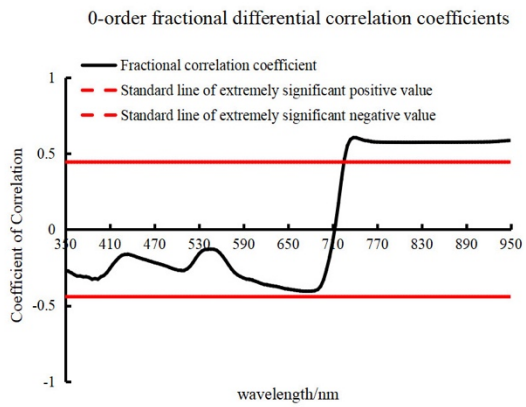

(a) 0-order fractional differential spectrum

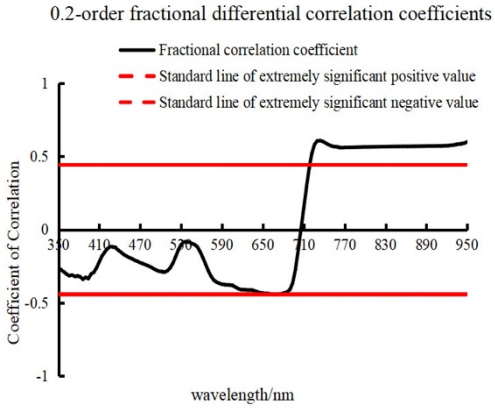

(b) 0.2-order fractional differential spectrum

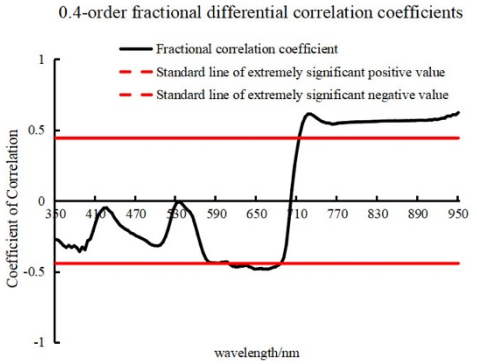

(c) 0.4-order fractional differential spectrum

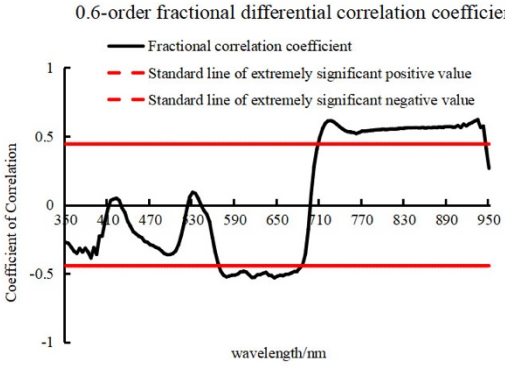

(d) 0.6-order fractional differential spectrum

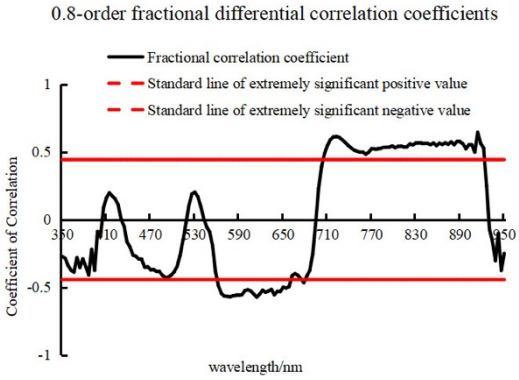

(e) 0.8-order fractional differential spectrum

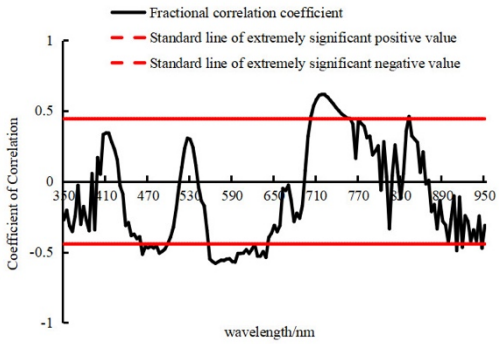

(f) 1.0-order fractional differential spectrum

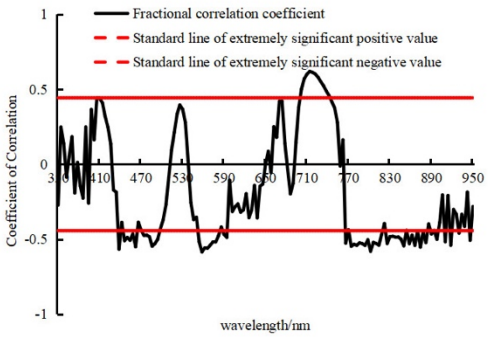

(g) 1.2-order fractional differential spectrum

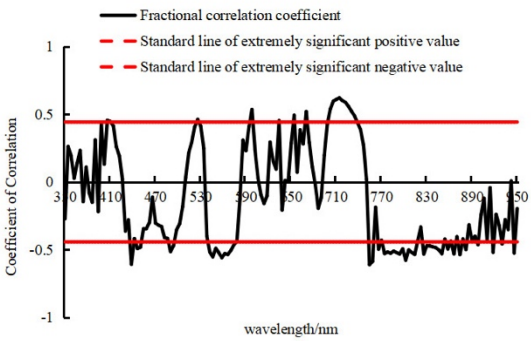

(h) 1.4-order fractional differential spectrum

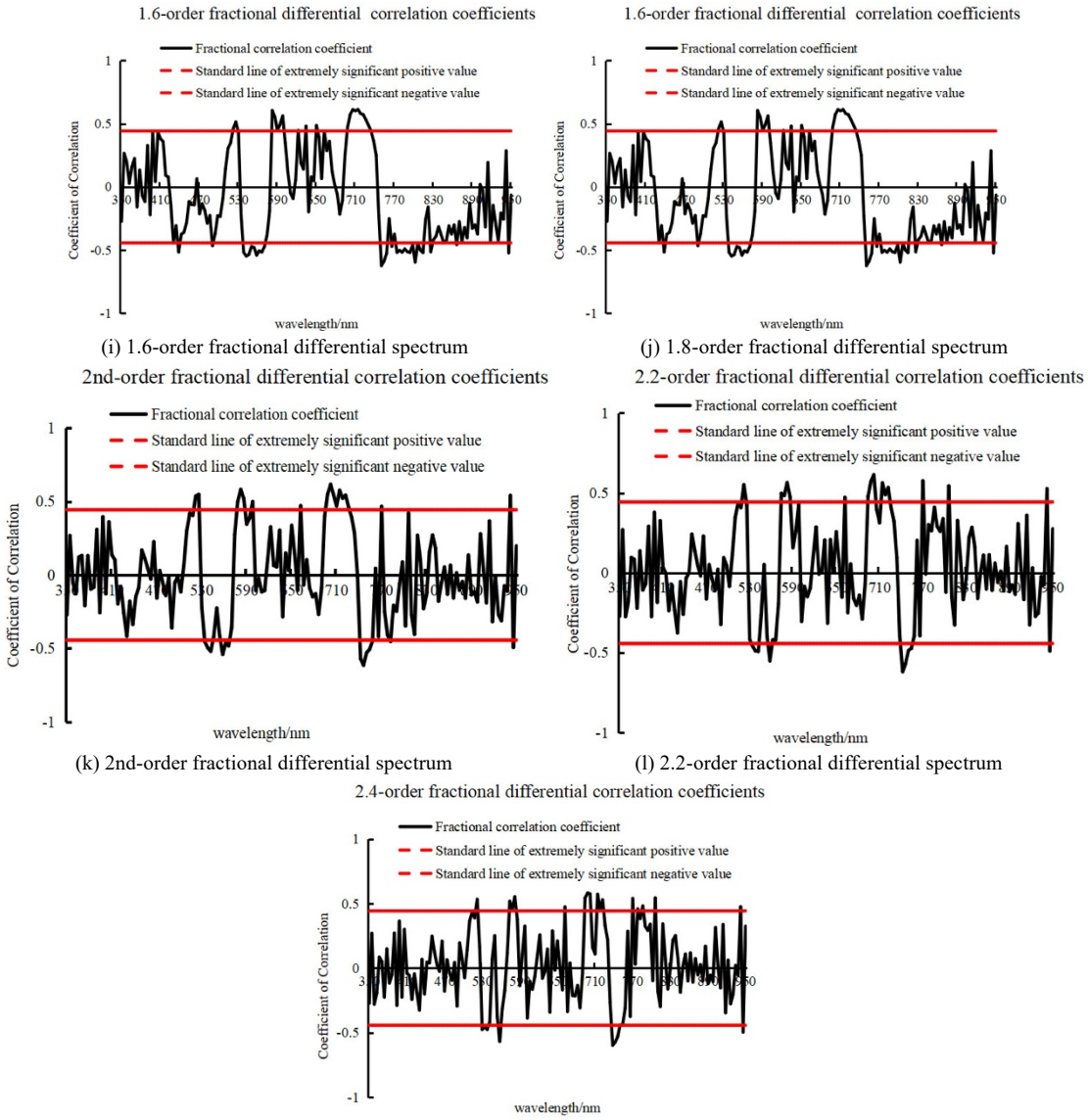

(i) 1.6-order fractional differential spectrum (j) 1.8-order fractional differential spectrum

(k) 2nd-order fractional differential spectrum (l) 2.2-order fractional differential spectrum

(m) 2.4-order fractional differential spectrum

Fig. 4. Correlation analysis between 0- and 2.4-order fractional differential spectra and winter wheat plant nitrogen content during the jointing stage

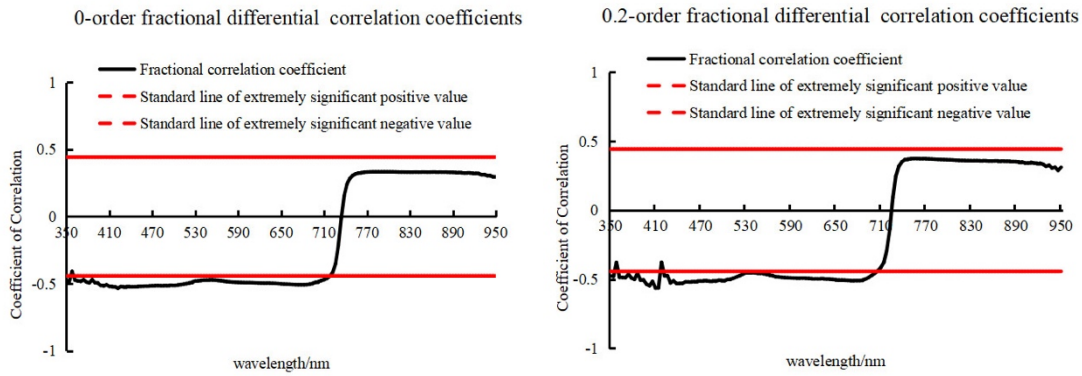

(a) 0-order fractional differential spectrum (b) 0.2-order fractional differential spectrum

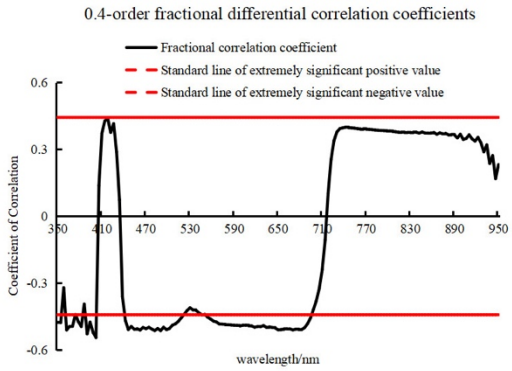

(c) 0.4-order fractional differential spectrum

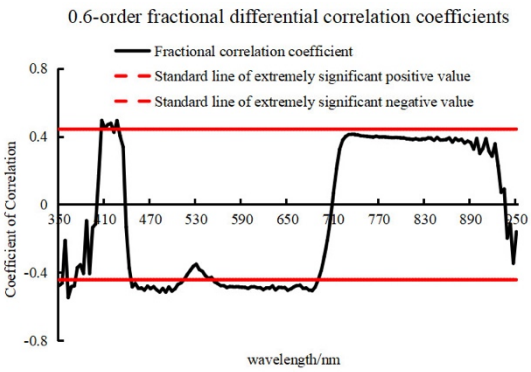

(d) 0.6-order fractional differential spectrum

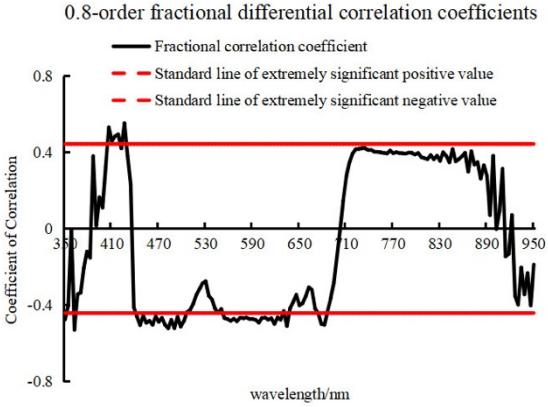

(e) 0.8-order fractional differential spectrum

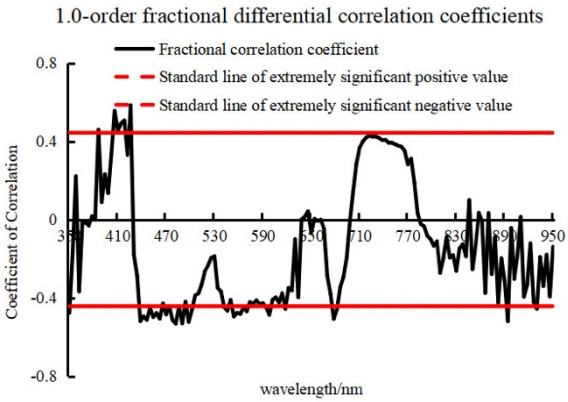

(f) 1.0-order fractional differential spectrum

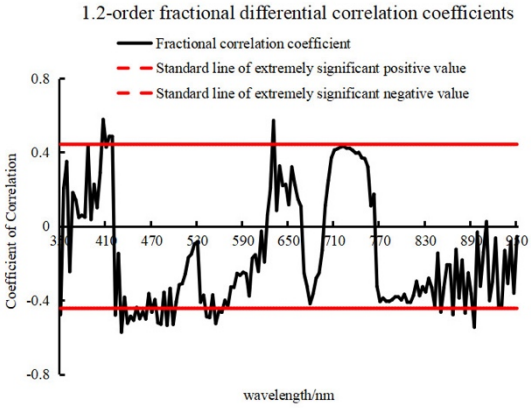

(g) 1.2-order fractional differential spectrum

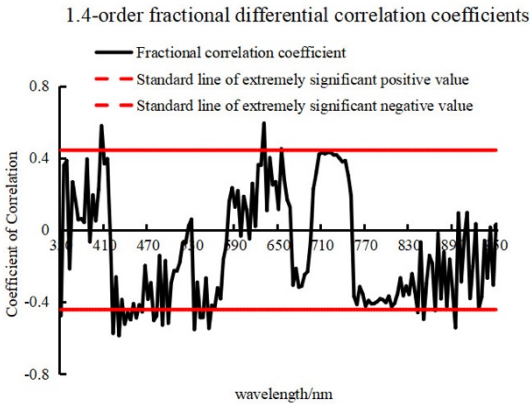

(h) 1.4-order fractional differential spectrum

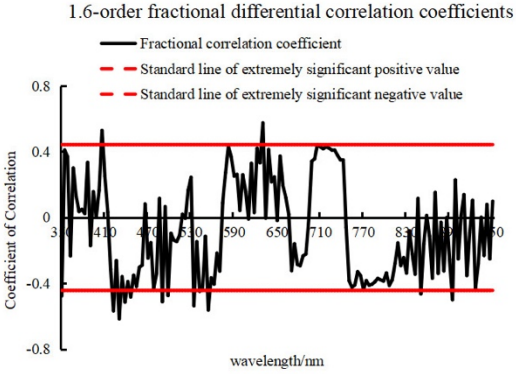

(i) 1.6-order fractional differential spectrum

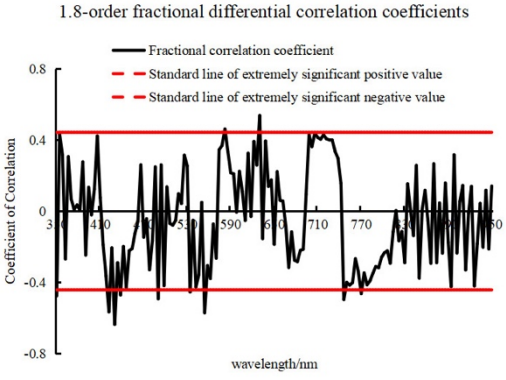

(j) 1.8-order fractional differential spectrum

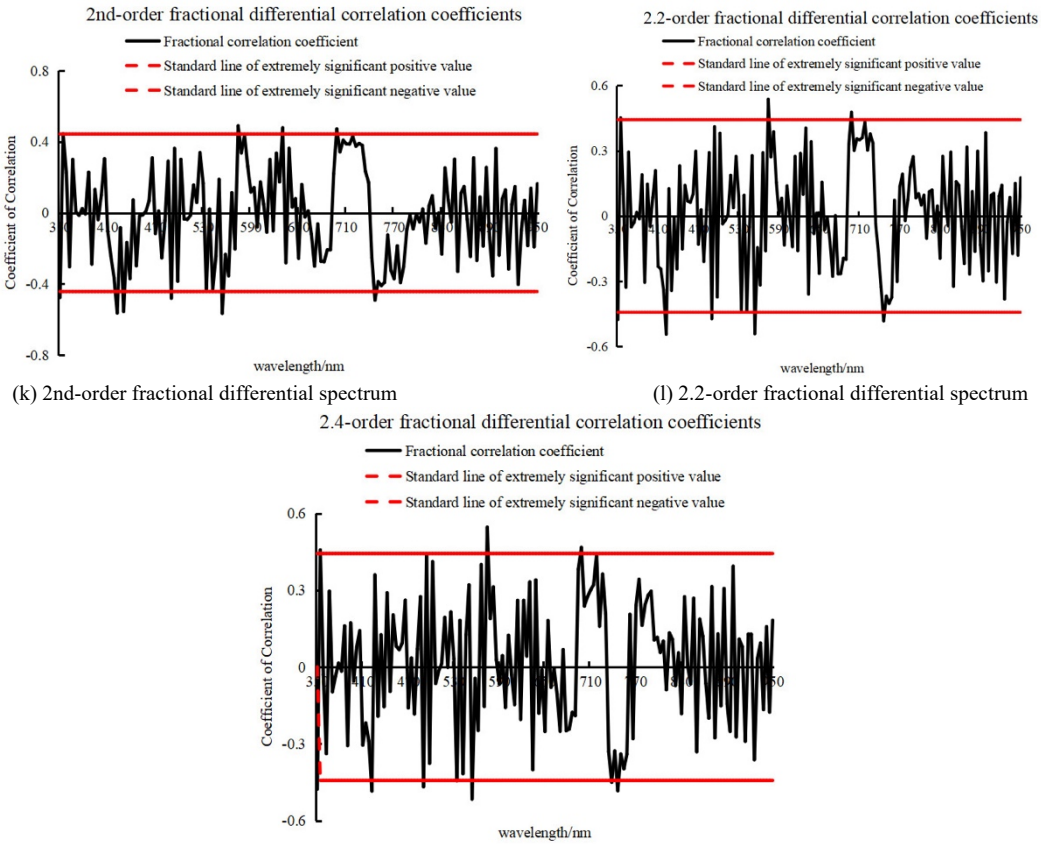

(k) 2nd-order fractional differential spectrum (l) 2.2-order fractional differential spectrum

(m) 2.4-order fractional differential spectrum

Fig. 5. Correlation analysis between the 0- and 2.4-order fractional differential spectra and nitrogen level of winter wheat plants during the filling stage

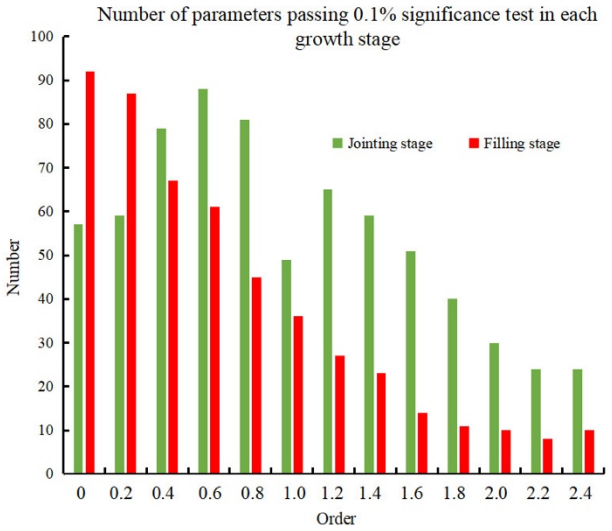

Fig. 6. Number of wavebands passing the 0.1% significance test at each growth stage

3.1.3 Comparison and optimization of sensitive characteristics of original and fractional canopy spectra with highly significant nitrogen content

The correlations of fractional differential and original canopy spectra with the winter wheat plant nitrogen content were assessed. On this basis, the wavebands (total: 13 bands) in which 0- to 2.4-order fractional differential spectra exhibited the strongest correlation with plant nitrogen content and the first 13 bands in which the original canopy spectrum revealed a correlation with plant nitrogen content at the jointing stage were extracted (Figure 7). The significance of the association between the spectra and winter wheat plant nitrogen content can be effectively enhanced by fractional differential processing of the original canopy spectra. The overall sensitivity of the maximum value of extreme significance of the fractional differential spectrum to plant nitrogen was elevated by 1.89%–4.89% in contrast to the sensitivity of the original canopy spectrum to plant nitrogen at the first 13 positions. The increase reached 3.43% and 3.23% in the first and second orders. Figure 8 presents the absolute values of the peak correlation coefficients between the fractional differential spectrum and plant nitrogen. A bimodal distribution was observed with a progressive increase in the order; it first increased and then decreased in the order range between 0 and 1. The maximum value appeared at 914 nm, corresponding to an order of magnitude of 0.8. The absolute value initially increased and subsequently decreased in the order range between 1.2 and 2.4. Furthermore, the maximum value (0.653) appeared at 746 nm, corresponding to 1.8. By comparing the significance of the original spectrum within the same band (Table 4), except for the slight reduction of 0.64% at a maximum of 738 nm corresponding to the order of 2.4, the significance level of the correlation with N% at other orders increased by approximately 1.66%–58.82% compared with the original spectrum. The improvement effect was the maximum at 714 nm, corresponding to the order of 1.4, reaching 58.82%.

Table 4. Maximum value of the absolute correlation coefficient between fractional differential spectra and plant nitrogen level at the jointing stage and the corresponding wavelength and increased amplitude

Order and corresponding wavelength	Absolute value of correlation coefficient	Original canopy spectrum	Absolute value of correlation coefficient	Increase amplitude
0-order max738	0.604	W738	0.604	0.00%
0.2-order max734	0.610	W734	0.592	1.87%
0.4-order max950	0.623	W950	0.589	3.44%
0.6-order max934	0.621	W934	0.581	4.03%
0.8-order max914	0.645	W914	0.576	6.94%
1-order max718	0.616	W718	0.174	44.23%
1.2-order max714	0.620	W714	0.033	58.66%
1.4-order max714	0.621	W714	0.033	58.82%
1.6-order max750	0.624	W750	0.590	3.36%
1.8-order max746	0.653	W746	0.597	5.60%
2-order max702	0.616	W702	0.263	35.34%
2.2-order max742	0.619	W742	0.603	1.66%
2.4-order max738	0.598	W738	0.604	−0.64%

Note: For example, the 0.2-order max734 item is the highest absolute correlation coefficient value between the 0.2-order fractional differential spectrum and N% and the corresponding wavelength of 734 nm.

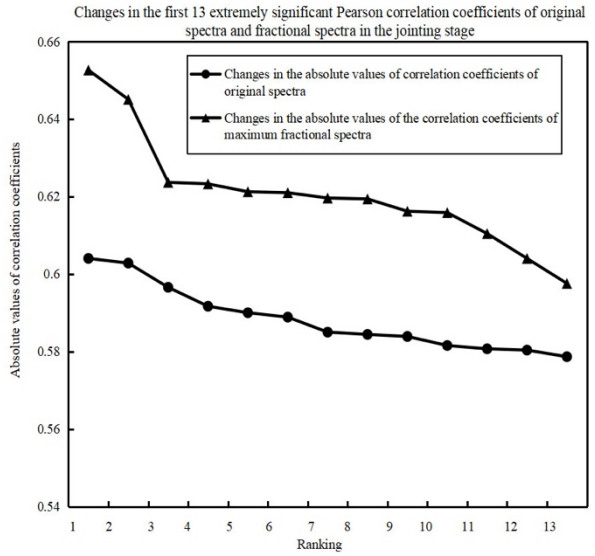

Fig. 7. Variation trend of the first 13 significant Pearson correlation coefficients between the original spectrum and fractional spectrum at the jointing stage.

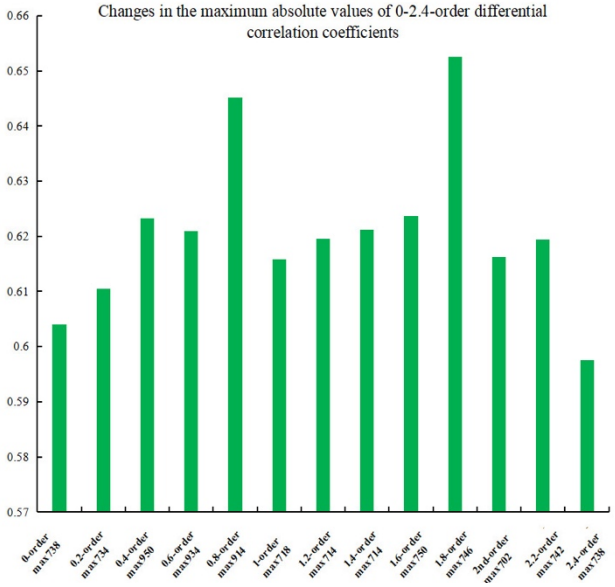

Fig. 8. Change in the maximum absolute 0- to 2.4-order differential correlation coefficient

The wavebands (total: 13 bands) in which the 0- to 2.4-order fractional differential spectra exhibited the highest correlation with plant nitrogen level and the first 13 bands in which the original canopy spectrum indicated a correlation with plant nitrogen level at the filling stage were extracted (Figure 9). The overall sensitivity of the maximum value of extreme significance of the fractional differential spectrum to plant nitrogen was elevated by 1.56%–10.27% in contrast to the sensitivity of the original canopy spectrum to plant nitrogen at the first 13 positions. The increase reached 5.93% and 4.18% in the first and second orders. Figure 10 shows the absolute value of the highest correlation coefficient between the fractional differential spectrum and plant nitrogen. A trimodal distribution was observed with a progressive increase in the order; it first increased and then decreased in the order range between 0 and 1. The maximum value appeared at 410 nm, corresponding to an order of 0.2 at 426 nm and an order of 1. In the order range between 1.2 and 2.4, the absolute value first increased and then decreased, increasing on the whole compared with the order range between 0 and 1. The absolute correlation coefficient at 430 nm corresponding to the order 1.8 was 0.637. Combining the significance of the original spectrum within the same band (Table 5), the absolute value of the highest correlation coefficient of integral fractional differential spectra with N% increased by nearly 0.99%–11.01% compared to the original spectrum. The improvement effect was the maximum at 430 nm, corresponding to 1.8, reaching 11.01%.

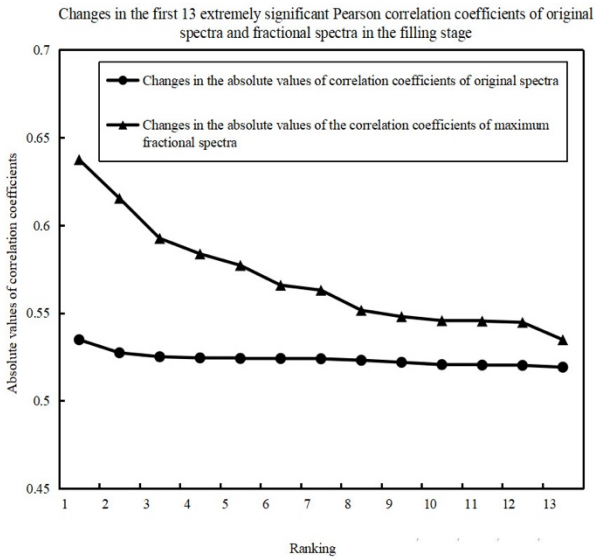

Fig. 9. Variation trend of the highly significant Pearson correlation coefficient between the original spectrum and fractional spectrum at the filling stage in the first 13 positions

Table 5. Maximum absolute correlation coefficient between the fractional differential spectrum and plant nitrogen content at the filling stage and the corresponding wavelength and increased amplitude

Order and corresponding wavelength	Absolute value of correlation coefficient	Original canopy spectrum	Absolute value of correlation coefficient	Increase amplitude
0-order max422	0.535	W422	0.604	0.00%
0.2-order max410	0.563	W410	0.592	4.25%
0.4-order max402	0.545	W402	0.589	2.63%
0.6-order max362	0.548	W362	0.581	7.45%
0.8-order max426	0.552	W462	0.576	2.85%
1-order max426	0.584	W462	0.174	6.07%
1.2-order max406	0.577	W406	0.033	6.82%
1.4-order max630	0.593	W630	0.033	9.63%
1.6-order max430	0.615	W430	0.590	8.81%
1.8-order max430	0.637	W430	0.597	11.01%
2-order max554	0.566	W554	0.263	9.26%
2.2-order max422	0.545	W422	0.603	0.99%
2.4-order max574	0.546	W574	0.604	6.00%

Note: For example, the 0.2-order max410 item is the highest absolute correlation coefficient value between the 0.2-order fractional differential spectrum and N% and the corresponding wavelength of 410 nm.

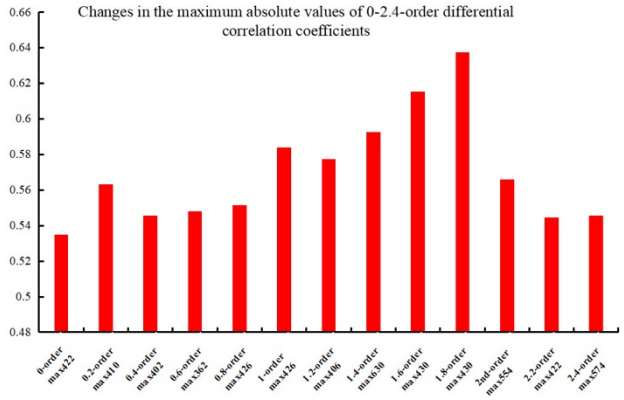

Fig. 10. Change in the maximum absolute 0- to 2.4-order differential correlation coefficient

In summary, the significance of the correlation between the spectra and nitrogen level of winter wheat plants can be effectively enhanced by fractional differential processing of the original canopy spectrum of winter wheat. The fractional differential wavelength corresponding to the highest absolute correlation coefficient between fractional differential spectra and winter wheat plant nitrogen level exhibited relatively optimal spectral characteristics.

3.2 Correlation analysis of hyperspectral vegetation index and spectral location and area characteristics with nitrogen content

3.2.1 Correlation analysis between the hyperspectral vegetation index and nitrogen content of winter wheat plants

The responsiveness of hyperspectral vegetation indices to the nitrogen level of winter wheat plants was evaluated by screening out the hyperspectral vegetation indices (Table 2 in Section 2.4.2) by a correlation coefficient test. Given the different biochemical components characterized by different vegetation indices, the correlation between them and the nitrogen level of winter wheat plants was extremely different. Figure 12a shows the results for the jointing stage. The absolute value of the correlation coefficients of the vegetation indices of NIR, R′, EVI, MSAVI2, R, OSAVI, FDOSAVI, FDDVI, FDNDVI, and B′ with the winter wheat plant nitrogen level ranged from 0.478 to 0.575, reaching a significant correlation level of 0.01. NIR and R′ were better than the other vegetation indices, reaching 0.575 and 0.561, respectively. This scheme can effectively characterize the winter wheat plant nitrogen level. The absolute values of the correlation coefficients of B, B′, G, FDNDVI, Carter6, OSAVI, EGFN, G′, R, and EVI with the winter wheat plant nitrogen level were between 0.448 and 0.517 (Figure 11b). The values reached the highly significant correlation level of 0.01. B and B′ were better than the other vegetation indices, reaching 0.517 and 0.502, respectively.

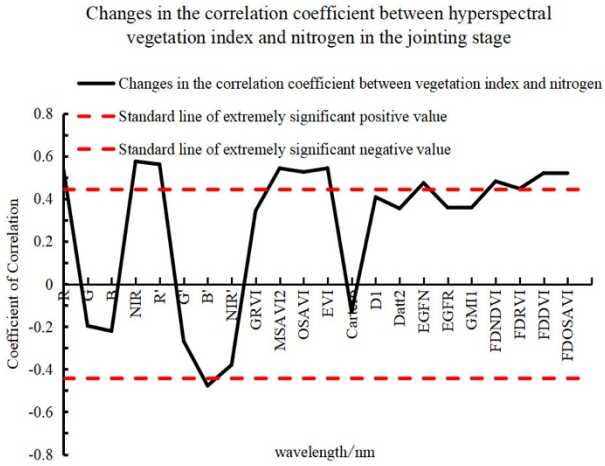

(a) Jointing stage

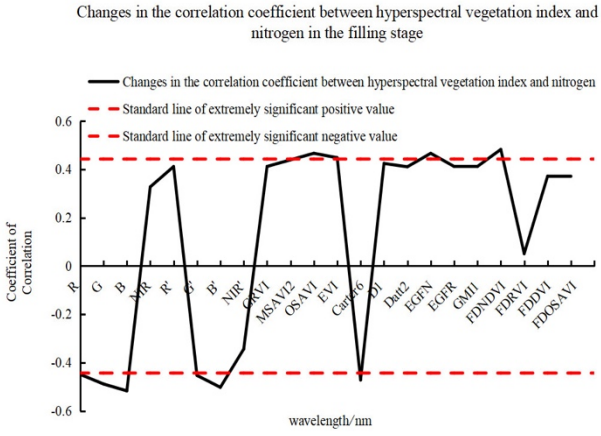

(b) Filling stage

Fig. 11. Changes in correlation coefficients between hyperspectral vegetation indices and nitrogen content

3.2.2 Correlation analysis of spectral position and area characteristics with winter wheat plant nitrogen content

The spectral characteristic distinguishing green plants from other surface features is the "red edge". Similarly, the "blue edge" and "yellow edge" exhibit similar characteristics to the red edge, and all of these edges are closely associated with the growth status of crops. As the "green peak" of the yellow light region is closely associated with chlorophyll and nitrogen, when crops are in a healthy growth stage, nitrogen is effectively absorbed, chlorophyll content is high, the green peak is partial to blue light, and the amplitude decreases. When crops are stressed by plant diseases and insect pests or "lose greenness" due to nitrogen deficiency, the green peak experiences a redshift, accompanied by an increasing amplitude. Hence, the nitrogen gains and losses of winter wheat during various growth periods can be explored by studying the spectral position and area characteristic parameters of winter wheat. Here, the responsiveness of spectral position and area characteristic parameters to the winter wheat plant nitrogen level was evaluated by screening out the spectral position and area characteristic parameters (Table 3 of Section 2.4.3) via the correlation coefficient test method. Figure 12a shows the trends for the jointing stage. The six characteristics are the yellow edge amplitude (D_y), yellow edge area (SD_y), red edge amplitude (D_r), red edge area (SD_r), and green peak position (λ_g). Furthermore, the standard value of the red and yellow edge area ((SD_r -SD_y)/ (SD_r +SD_y)) reached a high significance level of 0.01. The absolute values of the correlation coefficients were between 0.507 and 0.57, among which the green peak position (λ_g) and red edge area (SD_r)were better than the other characteristics, reaching 0.57 and 0.569, respectively. Figure 13b shows the trends for the filling stage. Seven characteristics, including the yellow edge amplitude (D_y), yellow edge position (λ_y), green peak reflectance(ρ_g), green peak area (SD_g), red valley reflectance (ρ_r), and normalized values of the red edge area and blue edge area ((SD_r - SD_b)/ (SD_r + SD_b)). The normalized values of the red edge area and yellow edge area((SD_r -SD_y)/ (SD_r +SD_y)) reached a level of 0.01. The absolute values of the correlation coefficients were between 0.445 and 0.508. Among them, red valley reflectance (ρ_r) and yellow edge amplitude (D_y) were better than other characteristics, reaching 0.508 and 0.504, respectively.

3.2.3 Screening of highly significant sensitive characteristics of nitrogen content in winter wheat plants

Based on the analytical findings presented in Sections 3.2.1 and 3.2.2, at the jointing stage, the relatively optimal sensitive characteristics with the highly significant responsiveness ranking top ten to winter wheat plant nitrogen content were NIR, green peak position (λ_g), red edge area (SD_r), R′ , yellow edge area (SD_y), red edge amplitude (D_r), EVI, MSAVI2, R, and yellow edge amplitude (D_y), and the absolute values of correlation coefficients were between 0.530 and 0.575 (Figure 13a). During the filling stage, the relatively optimal sensitive characteristics with the highly significant responsiveness ranking top ten to winter wheat plant nitrogen content were B, red valley reflectance (ρ_r), yellow edge amplitude (D_y), B′ , normalized values of red edge area and blue edge area ((SD_r - SD_b)/ (SD_r + SD_b)), G, green peak area (SD_g), FDNDVI, normalized values of red and yellow edge area ((SD_r - SD_y)/ (SD_r + SD_y)), and green peak reflectance (ρ_g). The absolute values of the correlation coefficients were between 0.475 and 0.517 (Figure 13b). Therefore, in this study, the ten vegetation indices or spectral position and area parameters reaching a highly significant correlation with the nitrogen content of plants were used as the characteristic input parameters for constructing the nitrogen content model of winter wheat plants.

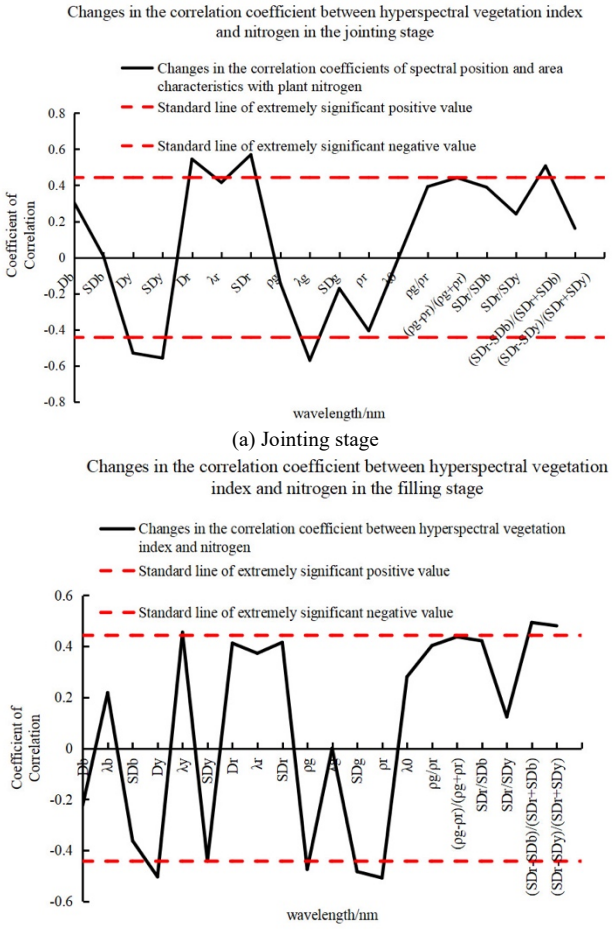

Fig. 12. Changes in correlation coefficients of spectral position and area with nitrogen content

3.3 Construction of an estimation model for winter wheat

3.3.1 Construction of plant nitrogen content model based on highly significant fractional differential spectra of plants

1) An estimation model for nitrogen content in winter wheat plants was developed through an all-subset regression analysis of R^2_{adj}

With the wavelength corresponding to the correlation analytical results between fractional differential spectra and nitrogen of winter wheat plants (Section 3.1.3) as the independent variable, a multilinear regression model of nitrogen content in winter wheat plants was constructed on the basis of all subset regression analyses of R^2_{adj} and evaluated by calculating R^2_{adj}, R^2, *RMSE*, and *nRMSE*. The RSS changes in all subset regression analyses during the jointing and filling stages are illustrated in Figures 14a and 14b. As the independent variable was added, the RSS of the model gradually decreased regardless of the jointing or filling stage. The optimal subset regression analytical results are shown in Figures 15a and 15b. Despite the data repetition of R^2_{adj} (y-coordinate), such as 0.54, 0.51, 0.56, and 0.58, under the same *nRMSE*, the smaller the number of

variables, the better (the same accuracy was reached using the minimal number of variables).

All subset regression analyses based on R^2_{adj} were performed. Then, a model was established using eight fractional spectral wavelengths, namely, 0-order (738 nm), 0.2-order (734 nm), 0.4-order (950 nm), 0.6-order (934 nm), 1.4-order (714 nm), 1.6-order (750 nm), 1.8-order (746 nm), and 2.4-order (738 nm) wavelengths, at the jointing stage and taken as independent variables. This subset model was optimal. Figure 15a displays the outcomes of the optimal subset analysis. Similarly, for the filling stage (Figure 15b), another model was constructed using ten fractional spectral wavelengths, namely, 0.2-order (410 nm), 0.4-order (402 nm), 0.6-order (362 nm), 0.8-order (426 nm), 1.0-order (426 nm), 1.2-order (406 nm), 1.6-order (430 nm), 1.8-order (430 nm), 2.0-order (554 nm), and 2.4-order (574 nm) wavelengths, and taken as independent variables. These variables represent the optimal subset model during the filling stage.

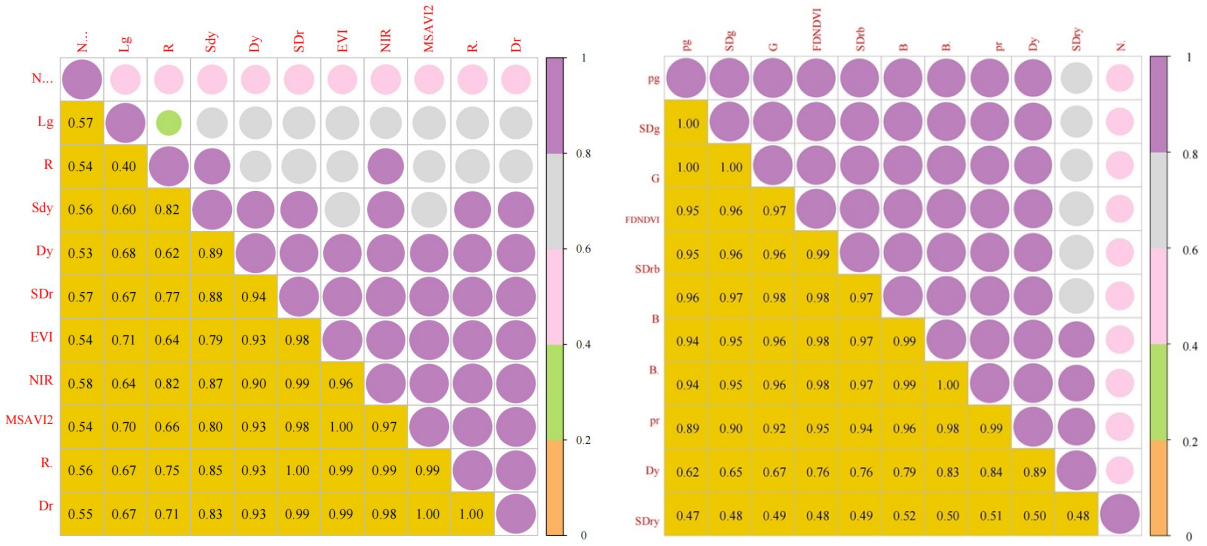

(a) Jointing stage (b) Filling stage

Fig. 13. Absolute values of the correlation coefficients of the top ten sensitive characteristics highly significantly correlated with plant nitrogen

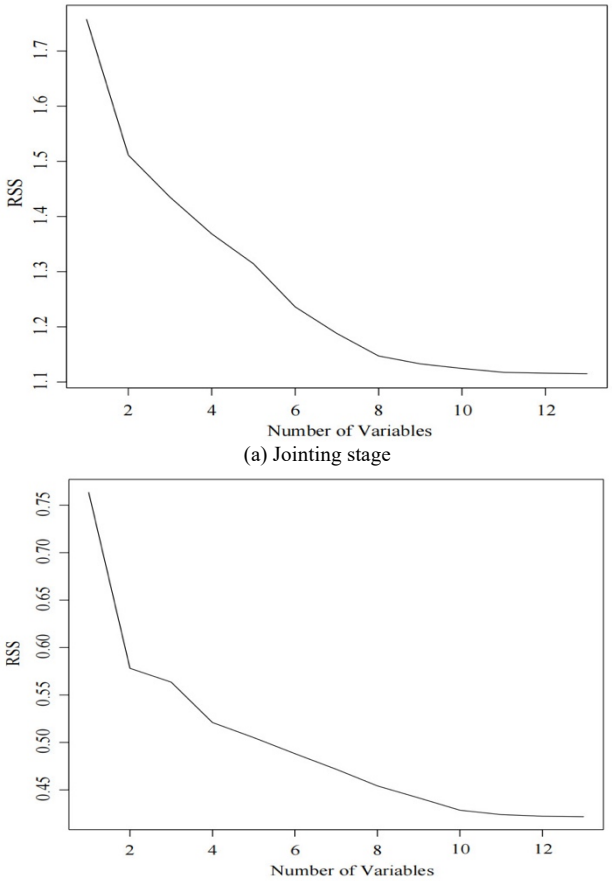

(a) Jointing stage

(b) Filling stage

Fig. 14. Change in the RSS of all subset regression analyses with the number of independent variables

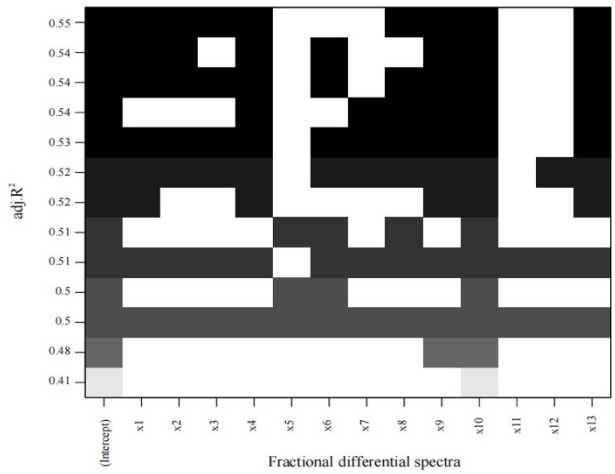

(a) Jointing stage

(Note: X1-X10 are the corresponding sensitive fractional spectra, namely, 0-order (738 nm), 0.2-order (734 nm), 2.4-order (738 nm), 0.6-order (934 nm), 0.8-order (914 nm), 1.0-order (718 nm), 1.2-order (714 nm), 1.4-order (714 nm), 1.6-order (750 nm), 1.8-order (746 nm), 2.0-order (702 nm), 2.2-order (742 nm), and 2.4-order (738 nm) spectra, at the jointing stage, which are also the independent variables of the model. The intercept is the model constant term. The correlation between the independent variable and R^2_{adj} increases as the color darkens. The white color denotes no correlation. In this study, with R^2_{adj} taken as the criterion, the black variables are screened out as independent variables to constitute the optimal subset.)

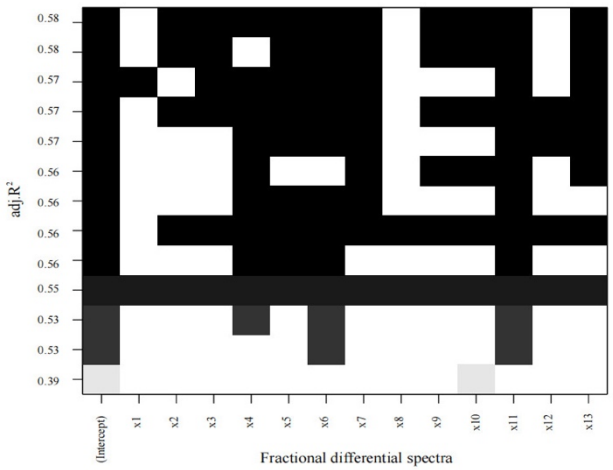

(b) Filling stage

(Note: X1–X10 is the corresponding sensitive fractional spectra, namely, 0-order (422 nm), 0.2-order (410 nm), 2.4-order (574 nm), 0.6-order (362 nm), 0.8-order (426 nm), 1.0-order (426 nm), 1.2-order (406 nm), 1.4-order (630 nm), 1.6-order (430 nm), 1.8-order (430 nm), 2.0-order (554 nm), 2.2-order (422 nm), and 2.4-order (574 nm) spectra, at the filling stage, which are also the independent variables of the model. The intercept is a constant term of the model.)

Fig. 15. All subset regression analyses of fractional differential spectra during the jointing and filling stages based on R^2_{adj}

2) The estimation model of nitrogen content in winter wheat plants was established by all subset regression analyses of the tenfold cross-validation

With the wavelengths corresponding to the correlation analytical results between fractional differential spectra and nitrogen content in winter wheat plants (Section 3.1.3) taken as the independent variables, a multilinear regression model of the nitrogen content in winter wheat plants was established on the basis of all subset regression analyses of the tenfold cross-validation and evaluated by calculating R^2_{adj}, R^2, *RMSE*, and *nRMSE*. All subset analyses were performed on the basis of tenfold cross-validation at each growth stage. Six fractional spectral wavelengths, namely, 0.6-order (934 nm), 1.2-order (714 nm), 1.4-order (714 nm), 1.6-order (750 nm), 1.8-order (746 nm), and 2.4-order (738 nm) wavelengths, at the jointing stage, were chosen as the independent variables for modeling. The minimum average cumulative deviation of the tenfold cross-validation is shown in Figure 16a. Similarly, for the filling stage (Figure 16b), the number of independent variables leading to the minimum average cumulative deviation of tenfold validation was 10. The analytical results of the independent variables used in this optimal subset model were ten fractional spectral wavelengths, namely, 0.2-order (410 nm), 0.4-order (402 nm), 0.6-order (362 nm), 0.8-order (426 nm), 1.0-order (426 nm), 1.2-order (406 nm), 1.6-order (430 nm), 1.8-order (430 nm), 2.0-order (554 nm), and 2.4-order (574 nm) wavelengths. The values coincide with all subset regression analyses based on R^2_{adj} results.

3.3.2 Construction of the plant nitrogen content model using highly significant sensitive spectral characteristics

1) Estimation model of winter wheat plant nitrogen content using all subset regression analyses of R^2_{adj}

With the ten sensitive spectral characteristics (i.e., vegetation index or spectral position and area parameters) previously optimized (Section 3.2.3) taken as independent variables, a multilinear regression model of nitrogen level in winter wheat plants was constructed on the basis of all subset regression analyses of R^2_{adj} and evaluated by calculating R^2_{adj}, R^2, *RMSE*, and *nRMSE*.

All subset regression analyses (Figure 16a) were performed on the basis of R^2_{adj}. At the jointing stage, a model was established by taking two sensitive spectral characteristics (green peak position (λ_g) and R) as independent variables. Similarly, for the filling stage (Figure 16b), a model was constructed using five sensitive spectral characteristics, namely, G, B, yellow edge amplitude (D_y), green peak area (SD_g), and red valley reflectance (ρ_r), and taken as independent variables. These variables represent the optimal subset model with sensitive spectral characteristics as the standard at the filling stage.

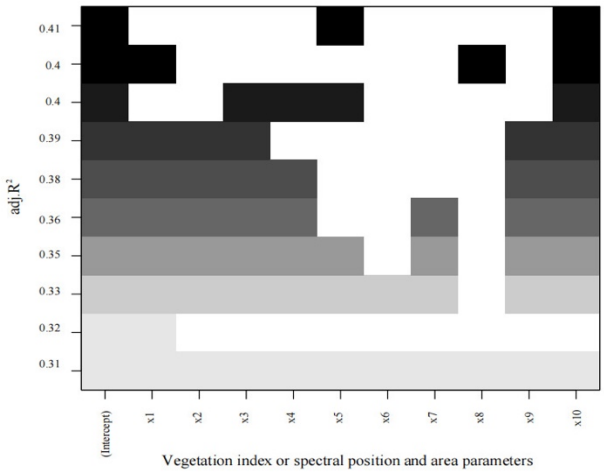

(a) Jointing stage

(Note: X1–X10 is the screened sensitive spectral characteristics at the jointing stage (Section 3.2.3), including NIR, green peak position (λ_g), red edge area (SD_r), R′, yellow edge area (SD_y), red edge amplitude (D_r), EVI, MSAVI2, R, and yellow edge amplitude (D_y), which are also the independent variables of the model. The intercept is a constant term of the model. The correlation between the independent variables and R^2_{adj} increases as the color darkens. The white color indicates no correlation. Here, the black-colored variables are independent variables screened on the basis of R^2_{adj} to form an optimal subset.)

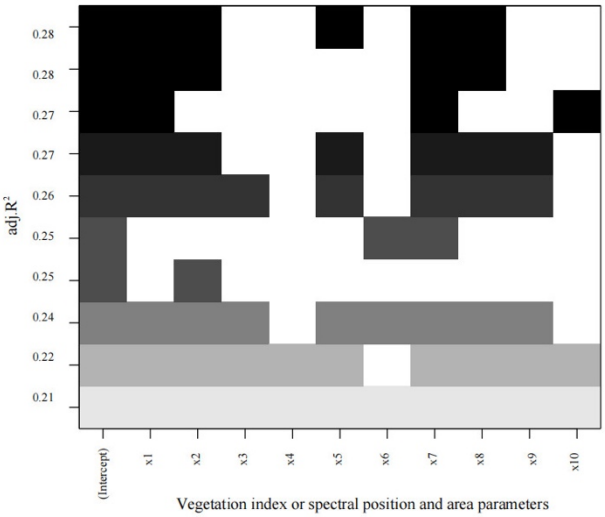

(b) Filling stage

(Note: X1–X10 is the screened sensitive spectral characteristics screened (Section 3.2.3), including B, red valley reflectance (ρ_r), yellow edge amplitude (D_y), B′, normalized values of red and blue edge area ((SD_r - SD_b)/(SD_r + SD_b)), G, green peak area (SD_g), FDNDVI, normalized values of red and yellow edge area ((SD_r - SD_y)/(SD_r + SD_y)), and green peak reflectance (ρ_g), which are also the independent variables of the model. The intercept is a constant term of the model.)

Fig. 16. All subset regression analysis of sensitive spectral characteristics based on R^2_{adj} during the jointing and filling stages

2) Estimation model of nitrogen level in winter wheat plants using all subset regression analyses of the tenfold cross-validation

Based on the correlation analytical results between sensitive spectral characteristics and nitrogen content in winter wheat plants (Section 3.2.3), a multilinear regression model of nitrogen level in winter wheat plants was constructed on the basis of all subset regression analyses of the tenfold cross-validation. All subset analyses were performed on the basis of tenfold cross-validation at each growth stage. At the jointing stage, two sensitive spectral characteristics (green peak position (λ_g) and R) were chosen as independent variables for modeling. The result was consistent with all subset regression analyses based on R^2_{adj}. In this case, the minimum average cumulative deviation of the tenfold cross-validation is shown in Figure 17a. Similarly, the average cumulative error increased as independent variables were added, showing an overall uptrend. Figure 17b shows the trends for the filling stage. In the case of only one independent variable, the average cumulative residual error was the minimum in all subsets, while that under other circumstances continued to increase. The analytical results of the independent variables used in this optimal subset model represented a single sensitive spectral characteristic, i.e., B.

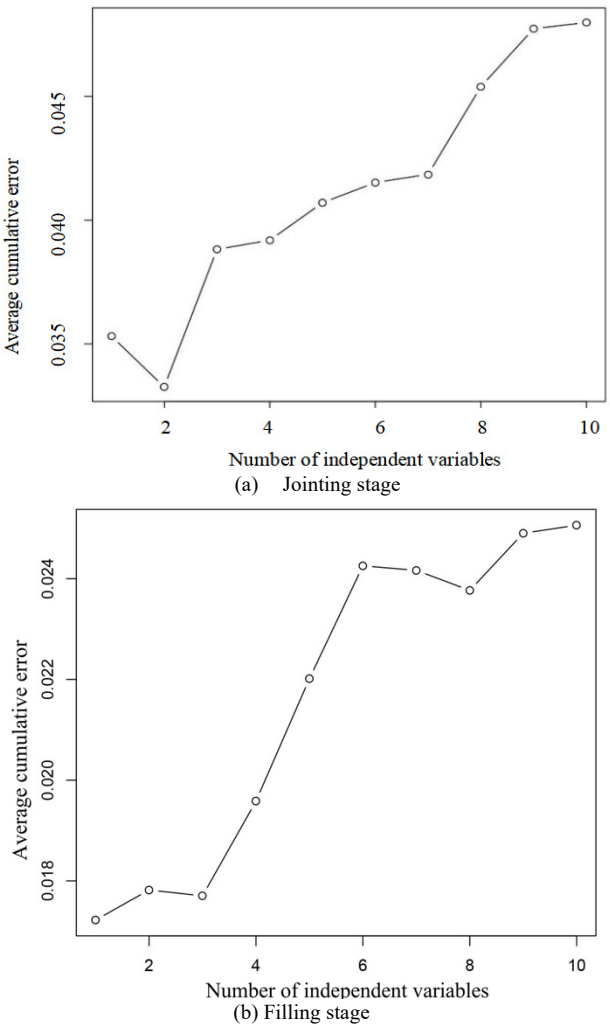

Fig. 17. Selection of independent variables for all subset regression analyses of sensitive spectral characteristics based on tenfold cross-validation

3.4 Model optimization and evaluation

The estimation models of nitrogen level in winter wheat plants established on the basis of the different spectral variables were evaluated and screened. Accordingly, a better estimation model was identified. The findings are shown in Table 6. The following findings can be inferred:

1) During the jointing stage, the R^2_{adj} and R^2 of the plant nitrogen content model using the fractional differential spectra increased by approximately 0.123 and 0.157 compared with those of the plant nitrogen level model on the basis of sensitive spectral characteristics, accompanied by an obvious reduction of *RMSE* and *nRMSE* by 2.9% and 0.94%, respectively. 2) At the filling stage, R^2_{adj} and R^2 of the plant nitrogen level model as fractional differential spectra increased by approximately 0.298 and 0.311 compared with those of the plant nitrogen content model based on sensitive spectral characteristics, accompanied by apparent reductions in *RMSE* and *nRMSE* by 3.7% and 2.75%, respectively. 3) At two typical growth stages of winter wheat, the plant nitrogen content model based on fractional differential spectra was generally better than that based on sensitive spectral characteristics. In contrast, R^2_{adj} and R^2 of the former were elevated. Furthermore, the corresponding *RMSE* and *nRMSE* values were significantly reduced, further proving that fractional differential spectra could highlight the minor differences between spectral data and improve the absorption of weak spectra to a great extent to save more valid information. 4) During the jointing stage, R^2_{adj} and R^2 of the optimal subset regression model established based on R^2_{adj} and fractional differential spectra increased by 0.011 and 0.029 compared with those of the optimal subset regression model using the tenfold cross-validation method. The *RMSE* and *nRMSE* values decreased by 0.5% and 0.19%, respectively. Meanwhile, the former showed a greater AIC than the latter. Moreover, as discussed in Section 3.3.1, the former included ten independent variables and six independent variables. The improvement was only minor because the model remained complex. Overall, the optimal subset regression model based on the tenfold cross-validation method was relatively optimal at the jointing stage. 5) At the filling stage, for models established on the basis of the fractional differential spectra, R^2_{adj}, R^2, *RMSE*, and *nRMSE*. The model parameters of the optimal subset regression model based on R^2_{adj} were relatively consistent with those of the optimal subset regression model using the tenfold cross-validation method.

In summary, in the two typical growth stages of winter wheat, the optimal subset regression model based on the tenfold cross-validation method with fractional differential spectra taken as variables was the relatively optimal estimation model for nitrogen content in winter wheat plants, as the model was validated while being optimally selected. The model validation results at two typical growth stages are presented in Figures 18a and 18b. Figure 18 shows the scattered points of plant nitrogen content predicted by the model and those of the actual measurements of the plant nitrogen content that were uniformly distributed near the 1:1 line.

Table 6. Accuracy evaluation of estimation models established on the basis of the different spectral variables at two typical growth stages

Growth stage	Modeling characteristic	Modeling method	Modeling accuracy				Validated accuracy			
			R^2	RMSE/ (%)	nRMSE	Adj. R^2	AIC	R^2	RMSE/ (%)	nRMSE
Jointing stage	Fractional differential spectrum	Adj. R^2	0.625**	0.155	5.04%	0.548**	−157.09	0.484*	0.185	6.12%
		tenfold cross-validation	0.596**	0.16	5.23%	0.537**	−157.97	0.596**	0.16	5.23%
	VI&D&SD# sensitive characteristic	Adj. R^2	0.439*	0.189	6.17%	0.414*	−144.4	0.289	0.267	8.82%
		tenfold cross-validation	0.439*	0.189	6.17%	0.414**	−144.4	0.439*	0.189	6.17%
Filling stage	Fractional differential spectrum	Adj. R^2	0.667**	0.094	6.99%	0.577**	−201.01	0.439**	0.095	7.12%
		tenfold cross-validation	0.667**	0.094	6.99%	0.577**	−201.01	0.439**	0.095	7.12%
	VI&D&SD# sensitive characteristic	Adj. R^2	0.356*	0.131	9.74%	0.279	−182.61	0.446°	0.12	8.97%
		tenfold cross-validation	0.267°	0.14	10.39%	0.251	−171.74	0.267°	0.14	10.39%

Note: VI in# is the hyperspectral vegetation index, and D&SD represents the characteristic based on spectral area and position; ° means the significance level of 0.1; * indicates the significance level of 0.05; ** denotes the extreme significance level of 0.01

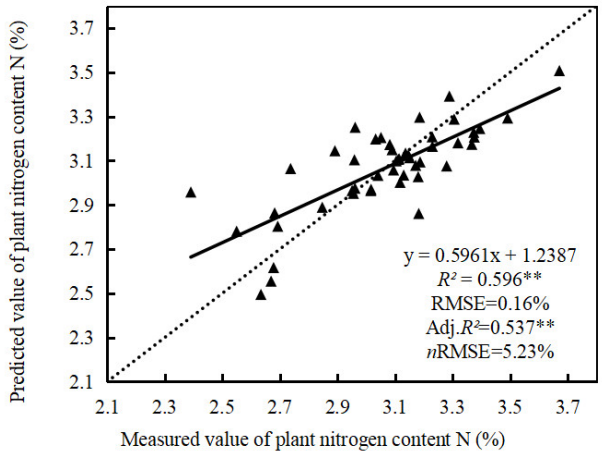

(a) Jointing stage

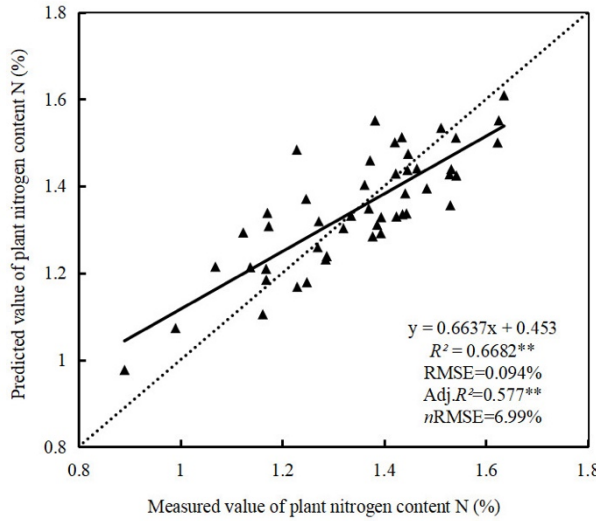

(b) Filling stage

Fig. 18. Validation of the optimal subset regression model based on the tenfold cross-validation method with fractional differential spectra as variables

4. Conclusions

The winter wheat canopies' UAV hyperspectral data underwent fractional differential processing in this study. The optimal fractional order reflecting plant nitrogen content and the wavelength were screened out on this basis. Meanwhile, the study compared the correlations between plant nitrogen content and hyperspectral vegetation indices, spectral location and area characteristic parameters. With highly significant spectral variables as the model input, optimal subset regression analysis was performed based on R^2_{adj} and tenfold cross-validation to establish relatively optimal estimation models for winter wheat plants at two typical growth stages: jointing and filling. On this basis, an experimental study was conducted. The study yielded the following conclusions:

1) After fractional differential processing, the original canopy spectrum can effectively enhance the correlation between spectral reflectance and nitrogen level in winter wheat plants. The corresponding wavelength was 714 nm, which represented an increase of 58.82% compared to the original canopy spectrum at the same wavelength., Furthermore, it exhibited a 1.89% increase compared with the maximum correlation coefficient observed in the canopy spectra and a 3.43% and 3.23% increase compared to the first and second-order spectra, respectively. During the filling stage, the maximum correlation coefficient was on the order of 1.8. The corresponding wavelength was 430 nm, with an increase of 11.01% compared with the original canopy spectrum of the same wavelength, 1.56% compared to the maximum correlation coefficient of the canopy spectra, and 5.93% and 4.18% compared with the first- and second-order spectra, respectively. These findings effectively prove that the fractional differential processing of canopy spectra can mitigate the impact of baseline shift and background noise and improve the spectral characteristics of physiological features inside winter wheat. These findings coincide with the study results of relevant scholars.

2) In the two typical growth stages of winter wheat, the nitrogen content model of the plant, utilizing fractional differential spectra, demonstrated superior performance compared to the model based on sensitive spectral characteristics. At the jointing and filling stage, R^2_{adj} and R^2 increased by approximately 0.123 and 0.157 and 0.298 and 0.311, respectively, accompanied by a significant reduction in *RMSE* by 2.9% and 0.94% and *nRMSE* by 3.7% and 2.75%, respectively. This finding further verified that fractional differential spectra had prominent effects on refining spectral details.

3) During the jointing stage, R^2_{adj} and R^2 of the optimal subset regression model established on the basis of R^2_{adj} and

fractional differential spectra increased by 0.011 and 0.029 compared with those of the optimal subset regression model using the ten-fold cross-validation method. Furthermore, the *RMSE* and *nRMSE* values decreased by 0.5% and 0.19%, respectively. Meanwhile, the former showed a greater AIC than the latter. The former included ten independent variables, four more than the latter. Therefore, this minor improvement was achieved despite the increase in model complexity. At the jointing stage, the optimal subset regression model based on fractional differential spectra and ten-fold cross-validation method was a relatively optimal model.

4) At the filling stage, for models established on the basis of fractional differential spectra, the optimal subset optimization results were consistent regardless of whether they were based on R^2_{adj} or ten-fold cross-validation. The same ten fractional spectral wavelengths were taken as the model input parameters.

This study demonstrates that the fractional differential processing of UAV hyperspectral data of winter wheat can effectively assess the nitrogen content in winter wheat plants, and it provides a feasible method for the scientific and precise management of nitrogen fertilizer prescription and the effective monitoring of plants' physiological growth status.

Acknowledgements

The authors are grateful for the support provided by the Scientific and Technological Research of Henan Province (Grant Nos. 232102320276 and 232400 411180) and the Scientific Research Program of the Department of Education of Henan Province (Grant No. 23B420003).

References

[1] L. Gao *et al*., "Winter wheat LAI estimation using unmanned aerial vehicle RGB-imaging," *Chin. J. Eco-Agr.*, vol. 24, no. 9, pp. 1254-1264, Oct. 2016.

[2] K. M. Dahlin, "Spectral diversity area relationships for assessing biodiversity in a wildland–agriculture matrix," *Ecol. Appl.*, vol. 26, no. 8, pp. 2758-2768, Dec. 2016.

[3] M. Du, N. Noguchi, A. Itoh, and Y. Shibuya, "Multi-temporal monitoring of wheat growth by using images from satellite and unmanned aerial vehicle," *Int. J. Agric. & Biol. Eng.*, vol. 10, no. 5, pp. 1-13, Sep. 2017.

[4] K. B. Byrd *et al.*,"Quantifying drought's influence on moist soil seed vegetation in California's Central Valley through remote sensing," *Ecol. Appl.,* vol. 30, no. 7, Oct. 2020, Art no. e02153.

[5] G. Walburg, M. E. Bauer, C. S. T. Daughtry, and T. L. Housley, "Effects of Nitrogen Nutrition on the Growth, Yield, and Reflectance Characteristics of Corn Canopies1," *Agron. J.,* vol. 74, no. 4, pp. 677-683, Jul. 1982.

[6] G. L. Bruland and R. A. MacKenzie, "Nitrogen Source Tracking with δ15N Content of Coastal Wetland Plants in Hawaii," *J. Environ. Qual*., vol. 39, no. 1, pp. 409-419, Jan. 2010.

[7] H. Aasen, J. Bendig, A. Bolten, S. Bennertz, M. Willkomm, and G. Bareth, "Introduction and preliminary results of a calibration for full-frame hyperspectral cameras to monitor agricultural crops with UAVs," in *ISPRS Technical Commission VII Mid-Term Symposium*, Istanbul, Turkey, September 29 - October 2, 2014, pp. 1-8.

[8] H. Yu, H. Wu, and Z. Wang, "Evaluation of SPAD and Dualex for In-Season Corn Nitrogen Status Estimation," *Acta Agron. Sin*., vol. 36, no. 5, pp. 840-847, May 2010.

[9] X. Zhou, "Study on rapid diagnosis and physiology and biochemistry indexes of nitrogen nutrition in tea plants (Camellia sinensis)," M.S. thesis, Dept. Tea Food Sci. Technol., Anhui Agriculture Univ., Hefei, China, 2012.

[10] A. M. Ali, H. S. Thind, S. Varinderpal, and S. Bijay, "A framework for refining nitrogen management in dry direct-seeded rice using GreenSeeker™ optical sensor," *Comput. Electron. Agric.*, vol. 110, pp. 114-120, Jan. 2015.

[11] C. Zhang and J. M. Kovacs, "The application of small unmanned aerial systems for precision agriculture: a review," *Precis. Agric*., vol. 13, no. 6, pp. 693-712, Dec. 2012.

[12] Y. Shi *et al*.,"Framework of SAGI Agriculture Remote Sensing and Its Perspectives in Supporting National Food Security," *J. Integr. Agr.*, vol. 13, no. 7, pp. 1443-1450, Jul. 2014.

[13] Y. Niu, L. Zhang, W. Han, and G. Shao, "Fractional Vegetation Cover Extraction Method of Winter Wheat Based on UAV Remote Sensing and Vegetation Index," *Trans. Chin. Soc. Agric. Eng*, vol. 49, no. 4, pp. 212-221, Mar. 2018.

[14] J. Yue *et al.*, "Estimation of Winter Wheat Above-Ground Biomass Using Unmanned Aerial Vehicle-Based Snapshot Hyperspectral Sensor and Crop Height Improved Models," *Remote Sens.*, vol. 9, no. 7, pp. 708, Accessed: 10 July, 2017. [Online]. Available: https://www.mdpi. com/2072-4292/9/7/708

[15] S. C. Kefauver *et al.*,"Comparative UAV and Field Phenotyping to Assess Yield and Nitrogen Use Efficiency in Hybrid and Conventional Barley," *Front. Plant Sci*., vol. 8, Oct. 2017, Art no. 1733.

[16] C. Liu *et al.*,"Nitrogen nutrition diagnosis of winter wheat based on ASD Field Spec3," *Trans. Chin. Soc. Agric. Eng*, vol. 34, pp. 162-169, Oct. 2018.

[17] K. Klem *et al.*,"Interactive effects of water deficit and nitrogen nutrition on winter wheat. Remote sensing methods for their detection," *Agric. Water Manage.,* vol. 210, pp. 171-184, Nov. 2018.

[18] K. Frels, M. Guttieri, B. Joyce, B. Leavitt, and P. S. Baenziger, "Evaluating canopy spectral reflectance vegetation indices to estimate nitrogen use traits in hard winter wheat," *Field Crops Res.,* vol. 217, pp. 82-92, Mar. 2018.

[19] S. Feng, T. Xu, F. Yu, C. Chen, X. Yang, and N. Wang, "Research of method for inverting nitrogen content in canopy leaves of Japonica rice in Northeastern China based on hyperspectral remote sensing of unmanned aerial vehicle," *Spectrosc. Spect. Anal.*, vol. 39, no. 10, pp. 3281-3287, Oct. 2019.

[20] L. Prey, Y. Hu, and U. Schmidhalter, "High-Throughput Field Phenotyping Traits of Grain Yield Formation and Nitrogen Use Efficiency: Optimizing the Selection of Vegetation Indices and Growth Stages," *Front. Plant Sci*., vol. 10, Jan. 2019, Art no. 1672.

[21] H. Liu, H. Zhu, Z. Li, and G. Yang, "Quantitative analysis and hyperspectral remote sensing of the nitrogen nutrition index in winter wheat," *Int. J. Remote Sens*., vol. 41, no. 3, pp. 858-881, Feb. 2020.

[22] R. R. Pullanagari, M. Dehghan-Shoar, I. J. Yule, and N. Bhatia, "Field spectroscopy of canopy nitrogen concentration in temperate grasslands using a convolutional neural network," *Remote Sens. Environ.*, vol. 257, May 2021, Art no. 112353.

[23] I. Tahmasbian, N. K. Morgan, S. Hosseini Bai, M. W. Dunlop, and A. F. Moss, "Comparison of Hyperspectral Imaging and Near-Infrared Spectroscopy to Determine Nitrogen and Carbon Concentrations in Wheat," *Remote Sens.*, vol. 13, no. 6, Mar. 2021, Art no. 1128.

[24] P. Hoang-Phi, T. Nguyen-Kim, V. Nguyen-Van-Anh, N. Lam-Dao, T. Le-Van, and T. Pham-Duy, "Rice yield estimation in An Giang province, the Vietnamese Mekong Delta using Sentinel-1 radar remote sensing data," *IOP Conference Series: Earth and Environmental Science*, vol. 652, no. 1, Feb. 2021, Art no. 012001.

[25] B. W. Burns, V. S. Green, A. A. Hashem, J. H. Massey, A. M. Shew, M. A. A. Adviento-Borbe, and M. Milad, "Determining nitrogen deficiencies for maize using various remote sensing indices," *Precis. Agric*., vol. 23, no. 3, pp. 791-811, Jun. 2022.

[26] P. Chen, "Retrieval Mechanism and Model Construction of Chlorophyll Content in Potato Based on Multi-source Remote Sensing of Unmanned Aerial Vehicle," M.S. thesis, Dept. Surv. Land Inform. Eng., Henan Polytechnic Univ., Jiaozuo, China, 2019.

[27] R. L. Whetton, K. L. Hassall, T. W. Waine, and A. M. Mouazen, "Hyperspectral measurements of yellow rust and fusarium head blight in cereal crops: Part 1: Laboratory study," *Biosyst. Eng*., vol. 166, pp. 101-115, Feb. 2018.

[28] R. Pu and P. Gong, "Hyperspectral remote sensing and its applications,"*Beijing, China: Higher Education Press*, 2003, pp. 66-70.

[29] C. Fu, S. Gan, X. Yuan, H. Xiong, and A. Tian, "Impact of Fractional Calculus on Correlation Coefficient between Available Potassium and Spectrum Data in Ground Hyperspectral and Landsat 8 Image," *Mathematics*, vol. 7, no. 6, May, 2019, Art no. 488.

[30] X. Wang, F. Zhang, H. Kung, and V. C. Johnson, "New methods for improving the remote sensing estimation of soil organic matter content (SOMC) in the Ebinur Lake Wetland National Nature Reserve (ELWNNR) in northwest China," *Remote Sens. Environ.*, vol. 218, pp. 104-118, Dec. 2018.

[31] K. Yasenjiang, S. T. Yang, T. Nigara, and F. Zhang, "Hyperspectral estimation of soil electrical conductivity based on fractional order differentially optimised spectral indices," *Acta Ecol. Sin.*, vol. 39, pp. 7237-7248, Aug. 2019.

[32] S. Rukeya *et al.*, "Spectral Estimation of Chlorophyll Content in Spring Wheat Leaves Based on Fractional Differential," *J. Triticeae Crops*, vol. 39, no. 6, pp. 738-746, May 2019.

[33] Y. Shi, W. Huang, J. Luo, L. Huang, and X. Zhou, "Detection and discrimination of pests and diseases in winter wheat based on spectral indices and kernel discriminant analysis," *Comput. Electron. Agric*., vol. 141, pp. 171-180, Sep. 2017.

[34] W. Ding, "Hyperspectral Remote Sensing Monitoring of Scab of Winter Wheat Based on Different Scales," M.S. thesis, Dept. Electron. Inform. Eng., Anhui Univ., Hefei, China, 2019.

[35] J. Jiang, Y. Chen, and W. Huang, "Using the Distance between Hyperspectral Red Edge Position and Yellow Edge Position to Identify Wheat Yellow Rust Disease," *Spectrosc. Spect. Anal.*, vol. 30, no. 6, pp. 1614-1618, Jun. 2010.

[36] J. Xu, X. Feng, L. Guan, S. Wang，and Q. Hu, "Fractional differential application in reprocessing infrared spectral data," *Control Instrum. Chem. Ind.*, vol. 39, no. 3, pp. 347-351, Mar. 2012.

[37] S. Dadras and H. R. Momeni, "Fractional-Order Dynamic Output Feedback Sliding Mode Control Design for Robust Stabilization of Uncertain Fractional-Order Nonlinear Systems," *Asian J. Control*, vol. 16, no. 2, pp. 489-497, Mar. 2014.

[38] G. Huang, L. Xu, and Y. Pu, "Summary of research on image processing using fractional calculus," *Appl. Res. Comput.*, vol. 29, no. 2, pp. 414-420, Feb. 2012.

[39] M. M. Saberioon, M. S. M. Amin, A. R. Anuar, A. Gholizadeh, A. Wayayok, and S. Khairunniza-Bejo, "Assessment of rice leaf chlorophyll content using visible bands at different growth stages at both the leaf and canopy scale," *Int. J. Appl. Earth Obs. Geoinf.*, vol. 32, pp. 35-45, Oct. 2014.

[40] G. Yang, "Investigation on Fractal Characteristics of Water System Extracted From Remotely-Sensed Imagery," M.S. thesis, Dept. Geogr. Inform. Eng. Cent., Southwest Jiaotong Univ., Chengdu, China, 2009.